Volume 5 | Number 18 | 14 May 2017 | Pages 4339–4586

Journal of Materials Chemistry C

Materials for optical, magnetic and electronic devices

rsc.li/materials-c

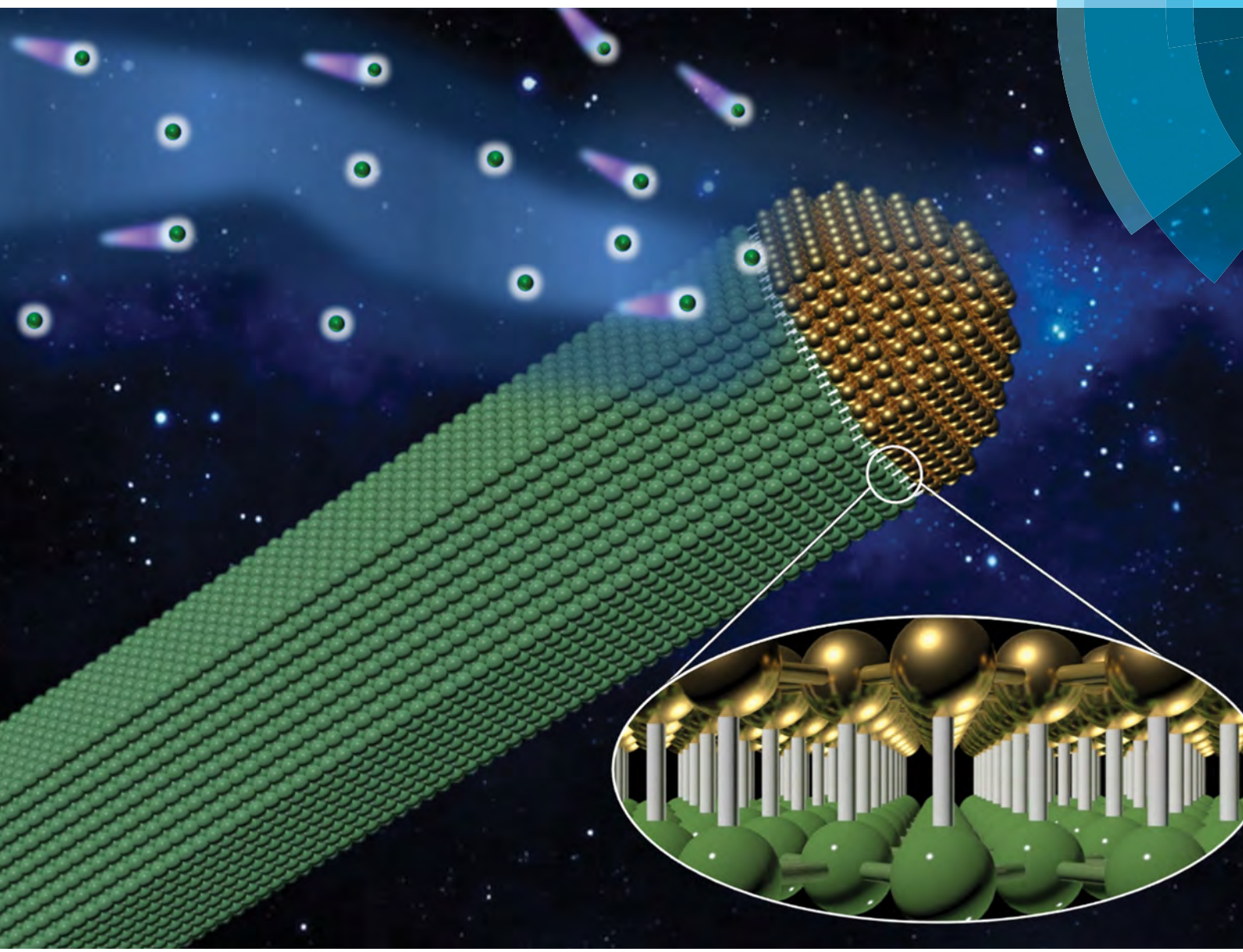

ISSN 2050-7526

ROYAL SOCIETY OF CHEMISTRY

PAPER

Zai-xing Yang, Johnny C. Ho *et al.*

Controllable III–V nanowire growth *via* catalyst epitaxy

Journal of Materials Chemistry C

PAPER

Cite this: J. Mater. Chem. C, 2017, 5, 4393

Controllable III–V nanowire growth *via* catalyst epitaxy†

Ning Han,[ab] Ying Wang,[ab] Zai-xing Yang,*[c] SenPo Yip,[de] Zhou Wang,[ab] Dapan Li,[d] Tak Fu Hung,[d] Fengyun Wang,[f] Yunfa Chen[ab] and Johnny C. Ho *[de]

Received 1st March 2017,
Accepted 27th March 2017

DOI: 10.1039/c7tc00900c

rsc.li/materials-c

Controllable synthesis of III–V compound semiconductor nanowires (NWs) with high crystallinity and uniformity is essential for their large-scale practical use in various technological applications, especially for those which are grown on non-crystalline substrates. In this study, the catalytic effect is investigated thoroughly in the growth of various III–V NWs in solid-source chemical vapor deposition, including Pd, Ag and Ni catalyzed GaAs NWs and Au catalyzed InGaAs and GaSb NWs. It is found that small diameter catalyst seeds lead to faster NW growth with better crystal quality, while large seeds result in slower NW growth with kinked morphology and twinning defects. Importantly, these small catalyst nanoparticles are observed to have higher solubility of the group III precursors due to the Gibbs–Thomson effect, which not only enables effective III precursor diffusion for a faster growth rate, but also yields epitaxial growth of NWs from the catalyst seeds accounting for the low activation energy and better crystallinity. All these results explicitly demonstrate the effectiveness of this catalyst solubility and epitaxy engineering for controlled III–V NW growth and indicate the potency for the reliable production of high-performance NWs for next-generation electronics.

Introduction

In recent years, owing to their superior carrier mobility and tunable bandgaps, III–V compound semiconductor nanowires (NWs) have been extensively explored as fundamental building blocks for next-generation electronics and optoelectronics.[1–5] Taking GaAs NWs as an example, a vertically standing single GaAs NW solar cell has demonstrated a record apparent efficiency of 40% over the Shockley–Queisser limit, illustrating their advantages in highly efficient and low-cost photovoltaics.[6] Generally, most NWs are synthesized epitaxially on single-crystalline substrates *via* the well-known vapor–liquid–solid (VLS) and/or vapor–solid–solid (VSS) growth mechanisms by both molecular beam epitaxy (MBE) and chemical vapor deposition (CVD). The epitaxial substrates play an important role in initiating the nucleation of NWs as well as dictating the NW growth orientations; however, the obtained NWs usually have mixed crystal phases and varied orientations even employing this epitaxial growth. This is mostly due to the fact that the hexagonal wurtzite phase would become more thermodynamically favorable in the nanometer scale as compared with the one of cubic zincblende such that NWs with different phases, orientations and even inversion domains are typically obtained.[7–9] All these would turn into more severe problems for the non-epitaxial growth of III–V NWs on amorphous substrates, such as on glass and SiO_2, in which the NW nucleation is more or less scattered and randomized.[10–12] Inevitably, non-epitaxial NW growth is preferred for high growth yield without underlying crystalline substrates in order to reduce the production cost for large-scale integration; as a result, it is highly desired to controllably synthesize III–V NWs with uniform growth behaviors and corresponding physical properties for technological applications.[12–15]

On the other hand, in addition to the substrate effect, the composition, size and phase of catalyst seeds are found to play an equally important role in directing the NW growth.[16–19] For example, Johanssan *et al.* found that a residual amount of In would allow GaAs NW growth with less defects as the NWs are actually catalyzed by Au–In alloy particles, instead of the

[a] State Key Laboratory of Multiphase Complex Systems, Institute of Process Engineering, Chinese Academy of Sciences, Beijing 100190, P. R. China
[b] Center for Excellence in Regional Atmospheric Environment, Institute of Urban Environment, Chinese Academy of Sciences, Xiamen 361021, P. R. China
[c] Center of Nanoelectronics and School of Microelectronics, Shandong University, Jinan 250100, P. R. China. E-mail: zaixyang@sdu.edu.cn
[d] Department of Physics and Materials Science, and State Key Laboratory of Millimeter Waves, City University of Hong Kong, Hong Kong SAR, P. R. China. E-mail: johnnyho@cityu.edu.hk
[e] Shenzhen Research Institute, City University of Hong Kong, Shenzhen 518057, P. R. China
[f] College of Physics and Cultivation Base for State Key Laboratory, Qingdao University, No. 308 Ningxia Road, Qingdao 266071, P. R. China

† Electronic supplementary information (ESI) available: SEM and TEM images of GaAs NWs catalyzed by Pd, TEM images and SAED patterns of InGaAs NWs catalyzed by Au. See DOI: 10.1039/c7tc00900c

conventional Au–Ga seeds,[19] and so do Au–Cd–Zn alloys in CdZnTe NW growth.[18] Also, Wang and his coworkers identified the solid-state growth mode (*i.e.* VSS) of Al catalyzed Si NWs,[20] while Garnett *et al.* observed a similar VSS growth mechanism of Pt catalyzed Si NWs,[21] with all these illustrating the distinct difference from the standard Au catalyzed VLS growth mode. Recently, much attention has been paid to the catalytic effect of the composition of Au seeds on NW growth because of the associated Gibbs–Thomson effect. Specifically, the non-linear relationship between the GaAs NW diameter and the Au seed dimension was attributed to the different Ga solubilities in varied sizes of Au particles.[22] Holmes *et al.* also found that faster Ge NW growth with better crystallinity could be achieved by using Au–Ge alloy seeds with a higher Ge composition.[23,24] This improvement was believed to be related to the lower Gibbs energy required for NW nucleation and growth in the highly supersaturated seeds. Nevertheless, even in typical Au catalyzed GaAs NW growth, the solid-state diffusion of Ga in the Au–Ga alloy seeds is observed, as revealed by the electron diffraction of the catalyst tip.[25] Moreover, by utilizing the surface X-ray diffraction technique, the interface layers of the Au catalyst in contact with the substrate are confirmed to exist in the quasi-solid phase, which play an important role in guiding the subsequent InP NW growth.[26] In this regard, the conventional VLS growth mechanism should be reconsidered to include and contrast the quasi-VSS mode, where the insight obtained may help to further understand the distinguishably different growth behaviors of NWs.

In our previous study, the thin GaAs NWs were found to grow epitaxially in the VSS mode from the Ni–Ga alloy seeds using Ni nanoparticles as the catalyst and the NW phase and orientation were highly dependent on those of the Ni–Ga solid alloys.[27] Also, when employing Au catalytic seeds, we observed that Au–Ga alloys with different compositions could lead to varied growth rate and density of GaAs NWs with different diameters and growth orientations caused by the Gibbs–Thomson effect.[28] In this study, we adopt different catalyst nanoparticles such as Pd, Ag and Ni for GaAs NW growth and at the same time used Au seeds for the growth of different NWs, including InGaAs and GaSb, in order to assess controllable III–V NW growth *via* the engineering of catalytic solubility and epitaxy. Surprisingly, the results clearly demonstrate that small-diameter catalyst seeds with high Ga solubility lead to single crystalline NW growth with a fast growth rate and preferred ⟨111⟩ orientation. In contrast, large-diameter catalyst seeds with a lower Ga composition yield a slow growth rate and defective NW growth, with varied growth orientations such as the ⟨110⟩ direction and even with kinked and curved NWs. The associated mechanism can be explained in terms of the epitaxial growth of NWs from their catalyst seeds in the quasi-VSS growth mode. All these findings explicitly indicate that the general growth control of III–V NWs can be easily attained by the manipulation of catalyst epitaxy *via* the precursor solubility for uniform and high-performance NW synthesis, which is ultimately essential for the realization of next-generation nanoelectronics.

Experimental

Here, GaAs, InGaAs and GaSb NWs are grown by solid-source CVD as reported previously.[4,29–31] Typically, GaAs powders (0.8 g, 99.999% purity) and Pd films are employed as the solid source and the catalyst, respectively, located in the upstream and downstream zones of a two-zone furnace. After being pumped down to ~2 mTorr, H_2 (99.99% purity, flow at 100 standard cubic centimeters per minute, sccm) is introduced into the system and the pressure is maintained at ~0.5 Torr. The Pd catalyst is firstly annealed into nanoparticles at 800 °C for 10 min and then cooled down to 600 °C for NW growth. Simultaneously, the GaAs powder zone begins to ramp up to 860 °C at a rate of ~80 °C min^{-1}. After a growth duration of 60 min, the system is cooled down to room temperature in H_2 atmosphere and the NWs are harvested by sonication in absolute ethanol for high resolution transmission electron microscopy (HRTEM, JEOL 6700F), selected area electron diffraction (SAED, Philips CM20), and the attached energy dispersive X-ray spectroscopy (EDS) characterization. The morphology of the NWs is also observed by using a scanning electron microscope (SEM, FEI/Philips XL30).

Results and discussion

In an attempt to obtain Pd–Ga and Ag–Ga alloy catalyst seeds with different Ga precursor solubilities, 0.1 nm and 6 nm thick Pd and Ag catalyst films are used for the GaAs NW growth. The typical GaAs NWs grown by Pd seeds are shown in Fig. 1. It is clear that the thin GaAs NWs with a diameter of ~10 nm are single crystalline oriented in the ⟨111⟩ growth direction as evidenced from Fig. 1a and b. And the catalyst/NW interface is identified as $PdGa_5$(123)|GaAs(311) though the NWs are growing along the ⟨111⟩ direction. As depicted in ESI,† Fig. S1, these NWs are very uniform in diameter (10–30 nm) with a length greater than 10 μm, and more importantly, the corresponding catalyst

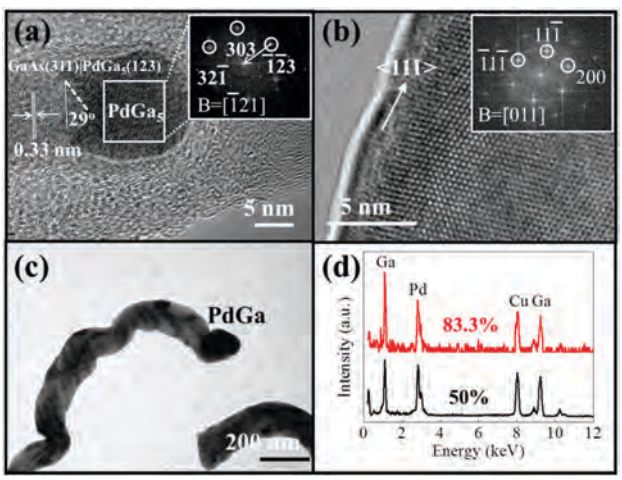

Fig. 1 GaAs NWs grown by using the Pd catalyst. (a and b) HRTEM images and the corresponding fast Fourier transformation (FFT) pattern of the thin GaAs NWs grown by using a 0.1 nm thick Pd film, (c) TEM image of the thick GaAs NWs grown by using a 6 nm Pd film, and (d) the EDS spectra of the Pd–Ga alloy seeds collected in (a) red and (c) black.

seed observed by HRTEM associated with the FFT pattern is identified to exist in the tetragonal $PdGa_5$ crystal phase. In contrast, the thick GaAs NWs are kinked with a very short length (~1 μm), as illustrated in Fig. 1c. The catalyst tip is identified to be PdGa from the EDS spectra (Fig. 1d) as compared with that of the small diameter $PdGa_5$ one. In this case, it is obvious that $PdGa_5$ seeds with a high Ga composition and small diameters can lead to highly crystalline GaAs NW growth with fast growth rates, which is in good agreement with the case of Au catalyzed GaAs NWs.[28] Although no obvious Ag–Ga catalyst tips are observed in the Ag catalyzed GaAs NWs as given in Fig. 2a and c, the thick NWs grown by using the 6 nm thick Ag film are heavily kinked with a large amount of defects (Fig. 2a), while the thin ones obtained by using the 0.1 nm thick Ag film are relatively straight and uniform (Fig. 2b) without any defect observed in the HRTEM image (Fig. 2d), implying a similar higher catalyst solubility effect in the small diameter Au seeds. And we also tried to synthesize GaAs NWs using a thick Ni catalyst apart from our previously used 0.5 nm Ni. However, a thicker Ni catalyst, such as 6 nm, cannot lead to NW growth, attributable to the higher eutectic temperature of Ni–Ga from the phase diagram than the Pd–Ga and Ag–Ga analogues. The thin GaAs NWs grown by using Ni are all highly crystalline, as we reported, in the ⟨111⟩ and ⟨110⟩ NW orientations,[25] and the unconventional ⟨311⟩ direction is also observed to grow by using the NiGa catalyst with an NiGa(211)|GaAs(311) interface as shown in Fig. 3.

Apart from GaAs NWs, we also attain GaSb NWs utilizing a 1 nm thick Au catalyst film, as illustrated in Fig. 4a and reported previously.[31] The NWs are rather thick with a diameter of ~200 nm and some are even defective, as shown in the SAED pattern in the inset of Fig. 4a. In contrast, very thin GaSb NWs can be grown with diameters down to 20 nm with improved crystallinity and a faster growth rate employing the sulfur-assisted growth method, as presented in Fig. 4b. In detail, the

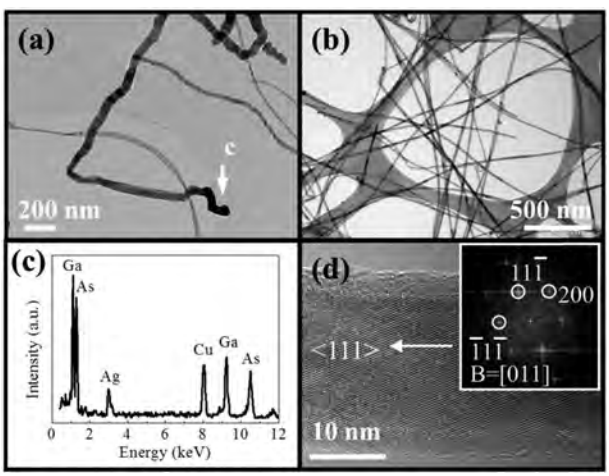

Fig. 2 GaAs NWs grown by using the Ag catalyst. (a and b) TEM images of the thick and thin GaAs NWs grown by using 6 and 0.1 nm thick Ag films, respectively, (c) the EDS spectrum of the catalyst tip collected in (a), and (d) the HRTEM image and corresponding FFT pattern of the thin GaAs NWs illustrated in (b).

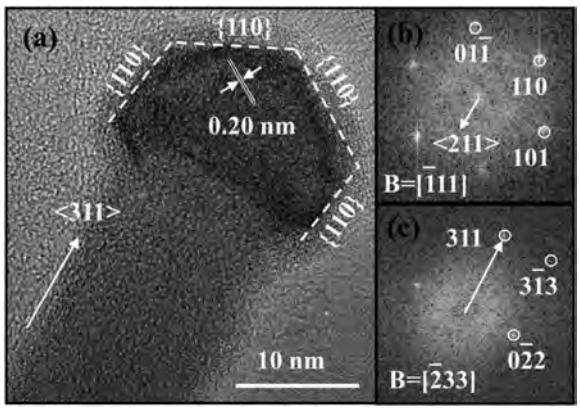

Fig. 3 GaAs NW grown by using a Ni catalyst with the NiGa(211)|GaAs(311) relationship. (a) HRTEM image of GaAs NWs and the polygonal catalyst, (b) and (c) FFT of the HRTEM images of the catalyst and the NW region.

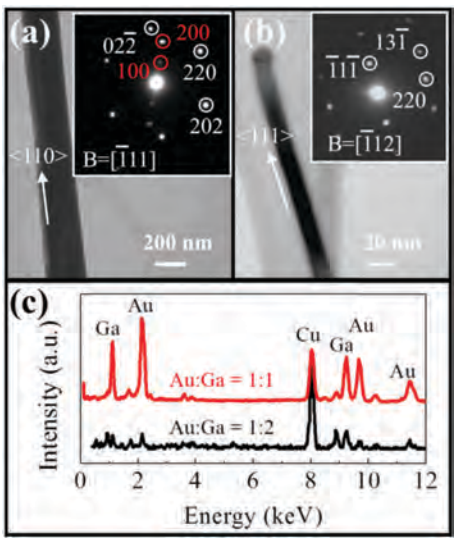

Fig. 4 GaSb NWs grown by using the Au catalyst. (a and b) TEM images and SAED patterns of typical thick NWs grown by using a 1 nm Au thick film and thin NWs grown by using a 0.1 nm thick Au film *via* the sulfur surfactant-assisted scheme, and (c) EDS spectra of the AuGa alloy seeds of the typical thick (red) and thin (black) GaSb NWs.

typical catalyst alloys are observed as AuGa for the thick NWs (200 nm) and $AuGa_2$ for the thin NWs (20 nm) as confirmed by the EDS studies given in Fig. 4c as well as the HRTEM images described in our previous work with $AuGa_2$(111)|GaSb(111) interface relationships.[4] These data assure again the effect of higher Ga solubility of the $AuGa_2$ catalyst alloy for highly crystalline GaSb NW growth, in good agreement with both the above-discussed GaAs NWs.

Furthermore, we also grow ternary InGaAs NWs by using a 2.5 nm thick Au catalyst film as shown in Fig. 5. It is evident that these NWs are heavily kinked (Fig. 5a) with a ⟨311⟩ high index growth orientation, as identified by the FFT of the HRTEM image (Fig. 5b). Typical twin defects (Fig. 5c) are also observed for the NWs grown in the ⟨111⟩ directions and a kinked angle of ~71° is often witnessed with the growth orientation changing

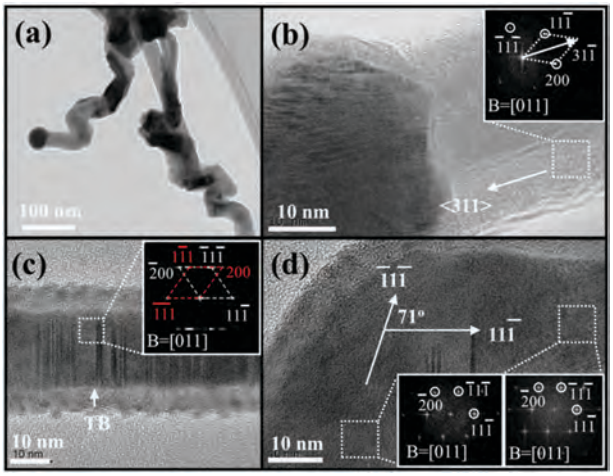

Fig. 5 InGaAs NWs grown by using the Au catalyst *via* the one-step growth method. (a) TEM image of the typical InGaAs NWs, (b) HRTEM image illustrating the crystal interface between the catalyst and the NW body, (c) and (d) typical twin-boundary (TB) defects and kinks observed in the NWs.

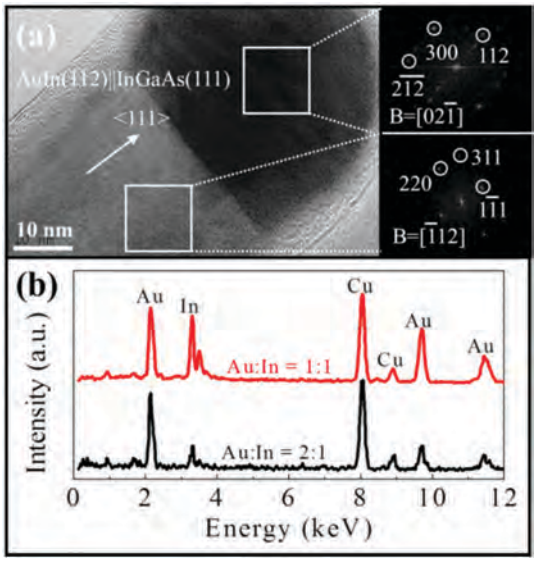

Fig. 6 InGaAs NW grown by using an Au film *via* the two-step method. (a) HRTEM image and corresponding FFT patterns of the AuIn alloy tips and InGaAs NW body, and (b) EDS spectra of the AuIn alloy tip collected in the one-step growth (black) and two-step growth (red) methods.

from [$\bar{1}1\bar{1}$] to [11$\bar{1}$] (Fig. 5d). And the kinked NWs with varied growth orientations are also illustrated in Fig. S2 in the ESI.† All these results explicitly indicate the poor crystallinity of the InGaAs NWs grown here. However, when we adopt a two-step growth method, that is before the NW growth, the Au catalyst nanoparticles are held at 600 °C for 2 min (GaAs and InAs mixed source powders are heated at 800 °C) for the effective nucleation of the NWs and then cooled down to 540 °C for the NW growth with all the other growth parameters unchanged, the NWs are grown with a much higher crystallinity and faster growth rate with a relatively smaller diameter, as depicted in Fig. 6 as well as in our previous report.[30] The InGaAs NWs are usually grown in the ⟨111⟩ directions, as identified from the FFT of the HRTEM image (Fig. 6a). Although the lattice of the catalyst tip is also observed in the HRTEM image, the FFT pattern cannot be indexed as any known Au_xGa_y or Au_xIn_y alloy phase. Interestingly, the Au_xGa_y and Au_xIn_y alloy phases exist in a very similar crystal structure as summarized in Table 1 because Ga and In are located in the same column in the periodic table with similar physical and chemical properties. In this case, if one assumes that the AuIn phase is in the same orthorhombic structure as the AuGa analogue, the FFT pattern can be identified well to be the AuIn phase with the lattice parameter 108% of the AuGa one with an AuIn(112)|InGaAs(111) interface. This is also proved by the EDS spectra showing that the AuIn alloy tips are composed of Au : In = 1 : 1 for the two-step growth method, but 2 : 1 for the one-step growth (Fig. 6b). Anyhow, all these findings again demonstrate clearly that single crystalline AuIn alloys with a higher In composition can grow InGaAs NWs faster and better (*i.e.* higher crystal quality) than the non-crystalline Au_2In alloy with a low In composition, which is in good agreement with the ones of GaAs and GaSb NWs.

It is noticeable that the InAs NWs grown by using the Au catalyst also contribute to similar results as illustrated by Zhang *et al.*[33] that the Au_xIn_y phase with higher In solubility (39 at%) would lead to crystalline InAs NW growth with faster growth rates as compared with the catalyst with a low In composition (16 at%). All the experimental data and the literature results are summarized in Table 2, where one can clearly see that the engineering of catalytic solubility is proved to be a general method for all the III–V NW growth control, with the possible extension to elemental NWs, such as Si and Ge, as reported in the literature,[23,34,35] demonstrating the promise of this catalyst controlled process for high-quality semiconductor NW growth. It is also noted that the NWs are grown in a uniform precursor feed without any precursor interruption, and also the NWs are cooled in their growth environment together with their source materials, which leads to a minimized post-growth phenomenon, as illustrated in many reports where Ga in the catalyst alloy is consumed by the As precursors if the Ga source is stopped firstly.[25,36,37] This is also proved by the absence of a neck region in the obtained NWs in our experiments, implying that most growth information is retained after being cooled down. Therefore, most of the growth information can be deduced from this post-growth analysis.

The growth rate difference can be first addressed considering the growth kinetics of NWs. In general, the growth procedure in MOCVD includes: (1) precursor decomposition at the catalyst surface, (2) dissolution and diffusion in the catalyst and (3) nucleation at the catalyst/NW interface, while in MBE, only steps (2) and (3) should be taken into consideration.[38–40] For the elemental NWs such as Si and Ge, the NWs are physically precipitated directly from the catalyst without any chemical reaction, and thus the growth rate is observed to be directly correlated with the supersaturation of the catalyst.[23,38] Specifically, the small diameter Au catalyst seeds can alloy more Ga or In precursor due to the Gibbs–Thomson effect ($\ln(C_d/C_0) = 4\gamma V_m/(dRT)$, where C_d is the concentration of Ga in Au nanoparticles with diameter d, C_0 is the equilibrium concentration

Table 1 Physical properties of different Au_xGa_y alloys extracted from the binary Au–Ga phase diagram[32] and comparison to our experimental results

Alloys	Crystal phase	Lattice constants (Å)	Ref.
$AuGa_2$	Cubic	$a = b = c = 6.073$	PDF3-0969
$AuIn_2$	Cubic	$a = b = c = 6.517$	PDF 3-0939
AuGa	Orthorhombic	$a = 6.266$, $b = 3.421$, $c = 6.399$	PDF 3-065-1488
AuIn	Orthorhombic	$a = 6.77$, $b = 3.69$, $c = 6.91$	AuGa x108%
$Au_{3.6}Ga_{0.4}$	Cubic	$a = b = c = 4.073$	COD1510527
$Au_{3.6}In_{0.4}$	Cubic	$a = b = c = 4.106$	COD1510528
GaAs	Cubic	5.653	PDF 12-0608
InAs	Cubic	6.0584	PDF 8-0387
GaSb	Cubic	6.095	PDF 7-0215
InSb	Cubic	6.4782	PDF 6-0208

Table 2 Influence of the catalyst supersaturation on the crystallinity of III–V NWs observed in this study and compiled in the literature

Catalyst/NW	Diameter (nm)	Supersaturation (atomic%)	Catalyst seed	Growth method	Crystallinity	Growth rate	Ref.
Au/GaAs	<20	50	AuGa	Single step SSCVD	Single crystalline	Fast	28 and 29
	~30	33.3	Au_2Ga	Single step SSCVD	Single crystalline	Fast	
	~40	30	Au_7Ga_3	Single step SSCVD	Single crystalline	Fast	
	50–200	22.2	Au_7Ga_2	Single step SSCVD	Multicrystalline	Low	
	~90	30–33.3	Au_7Ga_3, Au_2Ga	Two step SSCVD	Single crystalline	Fast	
Pd/GaAs	<20	83	$PdGa_5$	Single step SSCVD	Single crystalline	Fast	This study
	>100	50	PdGa	Single step SSCVD	Multicrystalline	Low	
Ag/GaAs	~20	NA	NA	Single step SSCVD	Single crystalline	Fast	This study
	~100	NA	NA	Single step SSCVD	Multicrystalline	Low	
Ni/GaAs	10–20	50–60	NiGa, Ni_2Ga_3	Single step SSCVD	Single crystalline	Fast	25
Au/InGaAs	20–100	33.3	Au_2In	Single step SSCVD	Multicrystalline	Low	This study
	50–70	50	AuIn	Two step SSCVD	Single crystalline	Fast	
Au/GaSb	~20	66.7	$AuGa_2$	Single step SSCVD, S assisted	Single crystalline	Fast	This study
	~200	50	AuGa	Single step SSCVD	Mixed	Low	
Au/InAs	<30	39	ε-Phase	MBE	Defect free	Fast	33
	>40	16	φ-Phase	MBE	Defected	Low	

in flat surface ($d \rightarrow \infty$) materials, γ is the surface energy, V_m is the molar volume of Au, R is a constant (8.314 J mol^{-1} K^{-1}), and T is the temperature[22,41]), and thus the supersaturation in small diameter catalysts is low leading to low growth rates of Si and Ge NWs. However, for most III–V compound NWs, only the III metal component is diffused from the catalyst, while the V elements come from the vapor phase because they are non-soluble in the catalyst.[10,25,42] In this case, the driving force for NW growth is not only the supersaturation of the catalyst, but also the exothermal chemical reaction at the interface which lowers the total energy of the system, as no Ga or In NWs have been obtained by the Au catalyst in the CVD system in the literature.

In our solid source CVD method, no organic precursor is used and thus only steps (2) and (3) control the growth rate of III–V NWs. Considering dissolution and diffusion, though the higher solubility of small diameter catalysts would reduce the precursor supersaturation, which is the driving force for NW growth, the resultant single crystalline catalyst alloy would favor precursor diffusion by providing both a short diffusion distance and uniform pathway as compared with non-crystalline large diameter catalysts. Also, the vapor phase V component will also diffuse more easily into the growth frontier in small diameter NWs compared with the large diffusion distance of the thick NWs. Quantitatively, if one considers the chemical reaction equation $v = A\exp(-E_a/RT)$ [III][V], where v is the reaction rate, E_a is the activation energy, A and RT are constants, and [III] and [V] denote the precursor concentration/pressure,[39] the higher solubility of Ga in the small diameter Au catalyst would increase the precursor concentration which would enhance the reaction rate. This is also in good agreement with the fact that for a high V/III growth ratio of III–V NWs, the [III] concentration would be the rate determining parameter,[39] and even in elemental NWs the growth rate is not only determined by the supersaturation but by the product of supersaturation and solubility.[38]

It is also worth noticing that besides tuning the solubility of the catalyst seeds, their corresponding crystal structures and phases would also be changed accordingly. As summarized in Table 2, the high solubility Au–Ga alloys are observed as AuGa, Au_7Ga_3 and Au_2Ga phases and even $AuGa_2$ for GaSb NWs, while the low solubility ones are present as Au_7Ga_2 for GaAs NWs. Even though they all occur in the hemisphere shape illustrating somewhat liquid phase properties, the interface layers are found to exist in a crystalline phase, which makes the VLS growth mechanism quasi-VSS.[25,26,43] Therefore, for investigating the effect of different crystal phases on the growth behavior of NWs, the interfacial atomic planes between the catalytic seeds and NWs are simulated as shown in Fig. 7. Notably, most of the GaAs, InGaAs and GaSb NWs prefer to grow along the ⟨111⟩ orientations, with the Ga/In atoms are aligned in the rhombus shape with a length of ~0.4 nm and an angle of 60°. The Ga alignments in the $AuGa_2$ (111) and NiGa (211) planes are exactly the same as the ones in GaSb (111) and GaAs (311),

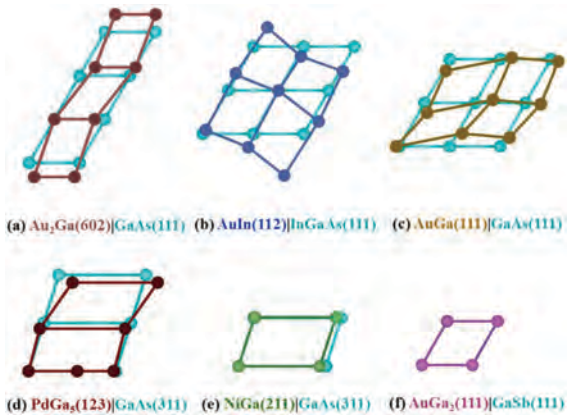

Fig. 7 Schematic view of the in-plane orientation of the catalytic seed and NW interfaces. (a) $Au_2Ga(602)|GaAs(111)$, (b) AuIn(112)|InGaAs(111), (c) AuGa(111)|GaAs(111), (d) $PdGa_5(123)|GaAs(311)$, (e) NiGa(211)|GaAs(311) and (f) $AuGa_2(111)|GaSb(111)$.

respectively, which would contribute effectively to the epitaxial growth of the GaSb (111) and GaAs (311) planes, as indicated in Fig. 7e and f. Although the Ga/In alignments in the Au_2Ga (602), AuIn (112) and AuGa (111) are not exactly the same as the one in GaAs (111) and InGaAs (111), respectively, they have the least mismatch, capable of epitaxy with minimal change in the interatomic distance or the interplanar angle, which would contribute efficiently to the ⟨111⟩ preferred growth orientation, as shown in Fig. 7a–c. This altered distance or angle could be the reason for the observed zone axis being not the same for both the catalyst tip and the NW body in many cases of GaAs NWs.[28] Moreover, it is also highlighted that the $PdGa_5$ catalyst would lead to a tilted growth frontier from the orientation, as shown in Fig. 1a, which may induce the epitaxial growth of NWs with the $PdGa_5(123)|GaAs(311)$ interface orientation, as given in Fig. 7c, leading to an angle of $\sim 29^\circ$ between the (311) growth plane and the ⟨111⟩ growth orientation. This phenomenon is also observed in Au_5Sn catalyzed SnTe NW growth.[44] As a result, the epitaxial growth of NWs from their catalyst tips would reduce the activation energy of the reaction of the III and V precursors at the interface, which accelerates the NW growth rate catalyzed by high III solubility Au seeds. It should be noticed that this reduced activation energy would play a more important role in the growth rate by the exponential relationship than only favoring the diffusion of precursors abovementioned. Furthermore, the catalyst epitaxial growth plays another important role in synthesizing highly crystalline NWs with preferred orientations similar to the MBE growth. Consequently, the epitaxial growth of III–V NWs by using high solubility catalysts plays the key role in growing single crystalline and unidirectional NWs with high growth rates, in good accordance with the literature that high crystal quality is accompanied by a high growth rate of NWs.[45,46]

Moreover, the catalytic solubility can be tailored by several viable means. First of all, the catalyst diameter can be made smaller in order to yield higher solubility as derived from the Gibbs–Thomson effect. The second way is to adopt a two-step growth scheme, as demonstrated in the case of GaAs and InGaAs NW growth, with an additional high-temperature step to obtain higher supersaturation in the initial stage of the NW nucleation.[28–30] The third one can be the formation of ternary alloy seeds for tuning the catalytic supersaturation, as illustrated in the ZnCdTe NW growth.[18] Last but not least, the utilization of a sulfur or oxygen surfactant assisted scheme can also minimize or even prohibit the Ostwald ripening of the catalyst particles during the NW growth; therefore, the particles can be upheld in a small size to maintain high solubility for the synthesis as observed in the cases of GaAs and GaSb NWs.[4,47,48] All these results illustrate the promising prospect of catalytic epitaxy engineering for well-controlled III–V NW growth for next-generation high-performance nanoelectronics.

Conclusions

In summary, for most III–V nanowires, including GaAs, InGaAs and GaSb, *etc.*, high solubility single crystalline catalyst alloys (*i.e.* Au–Ga, Pd–Ga, Ni–Ga and Au–In) will lead to a faster growth rate and higher crystal quality of the NWs as compared with those grown by low solubility non-crystalline catalysts. At the same time, the higher catalyst solubility will provide a fast precursor diffusion rate for NW growth, as well as more lattice-matched interfacial epitaxial layers for NW nucleation in a quasi-VSS mode which will reduce the activation energy for the precursor reaction at the interface and lead to NW growth. More importantly, the catalyst solubility and epitaxy effects can be well engineered by manipulating the catalyst size, growth and nucleation temperatures in the two-step growth scheme as well as implementing the surfactant-assisted growth in order to minimize the Ostwald ripening of the catalyst during NW synthesis. All these results clearly demonstrate the versatility of this catalyst solubility engineering in the III–V NW growth, which is also applicable to other NW systems, such as Ge, indicating the promising prospect of this technique in semiconductor NW growth for high-performance nanoelectronics and others.

Acknowledgements

This research was financially supported by the Early Career Scheme of the Research Grants Council of Hong Kong SAR, China (CityU 139413), the National Natural Science Foundation of China (Grants 51602314, 51672229 and 61504151), the State Key Laboratory of Multiphase Complex Systems (MPCS-2015-A-04), the CAS-CSIRO project of the Bureau of International Co-operation of Chinese Academy of Sciences (122111KYSB20150064), "Qilu young scholar" program of Shandong University, and the Science Technology and Innovation Committee of Shenzhen Municipality (Grant JCYJ20160229165240684), and was supported by a grant from the Shenzhen Research Institute, City University of Hong Kong.

Notes and references

1 J. A. del Alamo, *Nature*, 2011, **479**, 317–323.
2 M. S. Gudiksen, L. J. Lauhon, J. Wang, D. C. Smith and C. M. Lieber, *Nature*, 2002, **415**, 617–620.

3 K. Tomioka, M. Yoshimura and T. Fukui, *Nature*, 2012, **488**, 189–192.
4 Z. X. Yang, N. Han, M. Fang, H. Lin, H. Y. Cheung, S. P. Yip, E. J. Wang, T. F. Hung, C. Y. Wong and J. C. Ho, *Nat. Commun.*, 2014, **5**, 5249.
5 P. Caroff, K. Dick, J. Johansson, M. Messing, K. Deppert and L. Samuelson, *Nat. Nanotechnol.*, 2008, **4**, 50–55.
6 P. Krogstrup, H. I. Jorgensen, M. Heiss, O. Demichel, J. V. Holm, M. Aagesen, J. Nygard and A. F. I. Morral, *Nat. Photonics*, 2013, **7**, 306–310.
7 F. Glas, J. C. Harmand and G. Patriarche, *Phys. Rev. Lett.*, 2007, **99**, 146101.
8 H. Shtrikman, R. Popovitz-Biro, A. Kretinin, L. Houben, M. Heiblum, M. Bukała, M. Galicka, R. Buczko and P. Kacman, *Nano Lett.*, 2009, **9**, 1506–1510.
9 K. Ikejiri, Y. Kitauchi, K. Tomioka, J. Motohisa and T. Fukui, *Nano Lett.*, 2011, **11**, 4314–4318.
10 V. Dhaka, T. Haggren, H. Jussila, H. Jiang, E. Kauppinen, T. Huhtio, M. Sopanen and H. Lipsanen, *Nano Lett.*, 2012, **12**, 1912–1918.
11 N. Han, F. Y. Wang, A. T. Hui, J. J. Hou, G. C. Shan, F. Xiu, T. F. Hung and J. C. Ho, *Nanotechnology*, 2011, **22**, 285607.
12 N. Han, J. J. Hou, F. Wang, S. Yip, H. Lin, M. Fang, F. Xiu, X. Shi, T. Hung and J. C. Ho, *Nanoscale Res. Lett.*, 2012, **7**, 1–6.
13 K. A. Dick, K. Deppert, L. Samuelson, L. R. Wallenberg and F. M. Ross, *Nano Lett.*, 2008, **8**, 4087–4091.
14 H. J. Joyce, J. Wong-Leung, Q. Gao, H. H. Tan and C. Jagadish, *Nano Lett.*, 2010, **10**, 908–915.
15 Z. Y. Fan, J. C. Ho, T. Takahashi, R. Yerushalmi, K. Takei, A. C. Ford, Y. L. Chueh and A. Javey, *Adv. Mater.*, 2009, **21**, 3730–3743.
16 Y. S. Park, D. H. Jung, H. J. Kim and J. S. Lee, *Langmuir*, 2015, **31**, 4290–4298.
17 Y. S. Park, H. J. Kim and J. S. Lee, *Sci. Adv. Mater.*, 2016, **8**, 1696–1700.
18 H. Heo, K. Kang, D. Lee, L. H. Jin, H. J. Back, I. Hwang, M. Kim, H. S. Lee, B. J. Lee and G. C. Yi, *Nano Lett.*, 2012, **12**, 855–860.
19 J. Johansson, L. S. Karlsson, K. A. Dick, J. Bolinsson, B. A. Wacaser, K. Deppert and L. Samuelson, *Cryst. Growth Des.*, 2009, **9**, 766–773.
20 Y. W. Wang, V. Schmidt, S. Senz and U. Gosele, *Nat. Nanotechnol.*, 2006, **1**, 186–189.
21 E. C. Garnett, W. J. Liang and P. D. Yang, *Adv. Mater.*, 2007, **19**, 2946–2950.
22 G. Q. Zhang, K. Tateno, H. Sanada, T. Tawara, H. Gotoh and H. Nakano, *Appl. Phys. Lett.*, 2009, **95**, 123104.
23 C. O'Regan, S. Biswas, C. O'Kelly, S. J. Jung, J. J. Boland, N. Petkov and J. D. Holmes, *Chem. Mater.*, 2013, **25**, 3096–3104.
24 C. O'Regan, S. Biswas, S. Barth, M. A. Morris, N. Petkov and J. D. Holmes, *J. Mater. Chem. C*, 2014, **2**, 4597–4605.
25 A. I. Persson, M. W. Larsson, S. Stenstrom, B. J. Ohlsson, L. Samuelson and L. R. Wallenberg, *Nat. Mater.*, 2004, **3**, 677–681.
26 R. E. Algra, V. Vonk, D. Wermeille, W. J. Szweryn, M. A. Verheijen, W. J. P. van Enckevort, A. A. C. Bode, W. L. Noorduin, E. Tancini, A. E. F. de Jong, E. P. A. M. Bakkers and E. Vlieg, *Nano Lett.*, 2011, **11**, 44–48.
27 N. Han, A. T. Hui, F. Wang, J. J. Hou, F. Xiu, T. F. Hung and J. C. Ho, *Appl. Phys. Lett.*, 2011, **99**, 083114.
28 N. Han, F. Wang, J. J. Hou, S. Yip, H. Lin, M. Fang, F. Xiu, X. Shi, T. Hung and J. C. Ho, *Cryst. Growth Des.*, 2012, **12**, 6243–6249.
29 N. Han, J. J. Hou, F. Y. Wang, S. Yip, Y. T. Yen, Z. X. Yang, G. F. Dong, T. Hung, Y. L. Chueh and J. C. Ho, *ACS Nano*, 2013, **7**, 9138–9146.
30 J. J. Hou, N. Han, F. Wang, F. Xiu, S. Yip, A. T. Hui, T. Hung and J. C. Ho, *ACS Nano*, 2012, **6**, 3624–3630.
31 Z. X. Yang, F. Y. Wang, N. Han, H. Lin, H. Y. Cheung, M. Fang, S. Yip, T. F. Hung, C. Y. Wong and J. C. Ho, *ACS Appl. Mater. Interfaces*, 2013, **5**, 10946–10952.
32 T. Massalski, H. Okamoto, P. Subramanian and L. Kacprzak, *Binary Alloy Phase Diagrams*, ASM International, Materials Park, Ohio 44073, USA, 1990, vol. 3.
33 Z. Zhang, Z. Y. Lu, P. P. Chen, H. Y. Xu, Y. N. Guo, Z. M. Liao, S. X. Shi, W. Lu and J. Zou, *Appl. Phys. Lett.*, 2013, **103**, 073109.
34 B. Z. Tian, P. Xie, T. J. Kempa, D. C. Bell and C. M. Lieber, *Nat. Nanotechnol.*, 2009, **4**, 824–829.
35 S. A. Dayeh and S. T. Picraux, *Nano Lett.*, 2010, **10**, 4032–4039.
36 J. Harmand, G. Patriarche, N. Péré-Laperne, M. Mérat-Combes, L. Travers and F. Glas, *Appl. Phys. Lett.*, 2005, **87**, 203101.
37 D. Jacobsson, S. Lehmann and K. A. Dick, *Phys. Status Solidi RRL*, 2013, **7**, 855–859.
38 E. I. Givargizov, *J. Cryst. Growth*, 1975, **31**, 20–30.
39 C. Soci, X. Y. Bao, D. P. R. Aplin and D. L. Wang, *Nano Lett.*, 2008, **8**, 4275–4282.
40 C. Colombo, D. Spirkoska, M. Frimmer, G. Abstreiter and A. F. I. Morral, *Phys. Rev. B: Condens. Matter Mater. Phys.*, 2008, **77**, 155326.
41 D. R. Lide, *CRC handbook of chemistry and physics*, CRC press, Boca Raton, 2010.
42 S. K. Lim, S. Crawford, G. Haberfehlner and S. Gradecak, *Nano Lett.*, 2013, **13**, 331–336.
43 K. A. Dick, K. Deppert, T. Martensson, B. Mandl, L. Samuelson and W. Seifert, *Nano Lett.*, 2005, **5**, 761–764.
44 Y.-C. Zou, Z.-G. Chen, J. Lin, X. Zhou, W. Lu, J. Drennan and J. Zou, *Nano Res.*, 2015, **9**, 3011–3019.
45 M. Ramdani, E. Gil, C. Leroux, Y. André, A. Trassoudaine, D. Castelluci, L. Bideux, G. Monier, C. Robert-Goumet and R. Kupka, *Nano Lett.*, 2010, **10**, 1836–1841.
46 H. J. Joyce, Q. Gao, H. H. Tan, C. Jagadish, Y. Kim, M. A. Fickenscher, S. Perera, T. B. Hoang, L. M. Smith, H. E. Jackson, J. M. Yarrison-Rice, X. Zhang and J. Zou, *Nano Lett.*, 2009, **9**, 695–701.
47 N. Han, Z. Yang, F. Wang, S. Yip, G. Dong, X. Liang, T. Hung, Y. Chen and J. C. Ho, *ACS Appl. Mater. Interfaces*, 2015, **7**, 5591–5597.
48 S. Kodambaka, J. B. Hannon, R. M. Tromp and F. M. Ross, *Nano Lett.*, 2006, **6**, 1292–1296.